Hydrogen in energy and information sciences

Heejung W. Chung, Bernadette Cladek, Yong-Yun Hsiau, Yan-Yan Hu, Katharine Page, Nicola H. Perry, Bilge Yildiz, and Sossina M. Haile*

Beyond its fascinating chemistry as the first element in the Periodic Table, hydrogen is of high societal importance in energy technologies and of growing importance in energy-efficient computing. In energy, hydrogen has reemerged as a potential solution to long-term energy storage and as a carbon-free input for materials manufacturing. Its utilization and production rely on the availability of proton-conducting electrolytes and mixed proton–electron conductors for the components in fuel cells and electrolyzers. In computing, proton mediation of electronic properties has garnered attention for electrochemically controlled energy-efficient neuromorphic computing. Incorporation of substitutional and interstitial hydride ions in oxides, though only recently established, enables tuning of electronic and magnetic properties, inviting a range of possible exotic applications. This article addresses common themes in the fundamental science of hydrogen incorporation and transport in oxides as relevant to pressing technological needs. The content covers (1) lattice (or bulk) mechanisms of hydrogen transport, primarily addressing proton transport, but also touching on hydride ion transport; (2) interfacial transport; (3) exploitation of extreme external drivers to achieve unusual response; and (4) advances in methods to probe the hydrogen environment and transport pathway. The snapshot of research activities in the field of hydrogen-laden materials described here underscores exciting recent breakthroughs, remaining open questions, and breathtaking experimental tools now available for unveiling the nature of hydrogen in solid-state matter.

Science and technology drivers of the study of hydrogen in materials

As the first element in the Periodic Table, hydrogen holds a special place in chemistry. When incorporated as a component of solid-state matter, the unique features of hydrogen are particularly striking. Its light mass is comparable to the effective electron mass of some heavy-Fermion solids; dominant transport via tunneling at ambient temperatures is possible, with appreciable kinetic isotope effects; and it displays redox flexibility, occurring as a cation, as a neutral species, or as an anion, with dramatic differences in ionic/atomic radius, from effectively 0 in H^+, to 0.6 Å in H^0, and 1.1 Å in H^-. Furthermore, the hydride ion is far more polarizable than other anions of comparable ionic radius, O^{2-} and F^-, suggesting unusual bonding arrangements in hydride-bearing ionic solids. Beyond its

fascinating chemistry, hydrogen is of high societal importance in energy technologies and of growing importance in energy-efficient computing. In energy, hydrogen has re-emerged as a potential solution to long-term energy storage and as a carbon-free input for materials manufacturing. Perhaps the most relevant device in this context is the reversible protonic ceramic electrochemical cell, which interconverts between hydrogen for chemical energy storage and electricity for power delivery (**Figure 1**a).[1–3] In computing, proton mediation of electronic properties has garnered attention for electrochemically controlled energy-efficient neuromorphic computing. Here, the electrochemical synaptic device relies on proton intercalation into a channel material and the associated orders of magnitude change in electrical conductivity (Figure 1b).[4–6] Incorporation of substitutional and interstitial H^- in oxides, though only

Heejung W. Chung, Department of Materials Science and Engineering, Massachusetts Institute of Technology, Cambridge, USA; hjwchung@mit.edu
Bernadette Cladek, Department of Materials Science and Engineering, The University of Tennessee, Knoxville, USA; bcladek@utk.edu
Yong-Yun Hsiau, Department of Materials Science and Engineering, University of Illinois Urbana-Champaign, Urbana-Champaign, USA; yhsiau2@illinois.edu
Yan-Yan Hu, Department of Chemistry, Florida State University, Tallahassee, USA; yhu@fsu.edu
Katharine Page, Department of Materials Science and Engineering, The University of Tennessee, Knoxville, USA; kpage10@utk.edu
Nicola H. Perry, Department of Materials Science and Engineering, University of Illinois Urbana-Champaign, Urbana-Champaign, USA; nhperry@illinois.edu
Bilge Yildiz, Department of Materials Science and Engineering, Massachusetts Institute of Technology, Cambridge, USA; Department of Nuclear Science and Engineering, Massachusetts Institute of Technology, Cambridge, USA; byildiz@mit.edu
Sossina M. Haile, Department of Materials Science and Engineering, Northwestern University, Evanston, USA; sossina.haile@northwestern.edu
*Corresponding author
doi:10.1557/s43577-024-00714-9

recently established, enables tuning of electronic and magnetic properties (Figure 1c), inviting a range of possible exotic applications.[7] This article addresses common themes in the fundamental science of hydrogen incorporation and transport in oxides as relevant to pressing technological needs, recognizing lessons that can be learned from hydrides. The content covers (1) lattice (or bulk) mechanisms of hydrogen transport, primarily addressing proton transport, but also touching on hydride ion transport; (2) interfacial transport; (3) exploitation of extreme external drivers to achieve unusual response; and (4) advances in methods to probe the hydrogen environment and transport pathway.

Hydrogen transport refers to both diffusivity and conductivity, where the latter depends on both the concentration and mobility of charged species. As noted, because of its technological relevance in energy devices, lattice proton conductivity, and to some extent diffusivity, has been extensively studied, providing rich literature from which to draw conclusions. Hydride ion transport, in contrast, has only recently been reported, with relatively few studies of this phenomenon.

In proton-bearing ionic solids, the proton is tightly localized to a host, or "donor" species and creates a hydrogen bond between the donor and an acceptor species. Both donor and acceptor are often oxygen ions. Unlike other ions, a proton does not have its own electron cloud, so it is embedded in the valence shell of the donor.[8] A typical O–H bond distance is 1.1 Å, whereas the ionic radius of oxygen is ~1.4 Å. Bulk proton transport in most lattice conductors occurs via the Grotthuss mechanism,[9] as opposed to a vehicle mechanism in which a larger molecular ion carries the proton.[10] In the first step of the Grotthuss mechanism, the proton hops from its donor oxygen to a nearby acceptor oxygen. Because this requires the proton to be pulled out of the valence shell of the donor and into that of the acceptor, this transfer is facilitated when there is a significant overlap between the donor and acceptor electron clouds. In the second step, the lattice rearranges to bring the proton away from the donor. This step is necessary to enable long-range conduction by preventing back-and-forth shuttling between the donor and acceptor. The specific mechanisms and rates of these steps depend on the class of proton conductor.

The mechanisms of hydride ion transport can be presumed to be similar to those of other anion conductors, with the caveat that additional anionic species, in particular O⁻, may exist in the structure, impacting the H⁻ diffusion pathway.

Classes of lattice proton conductors

Two primary categories of technologically relevant lattice proton conductors are known. These are the solid acids, which include protons as part of their crystalline structure,[11–13] and hydrated ternary metal oxides, which incorporate protons via dissociative absorption of H_2O in the form of OH^- and H^+.[14–16] Beyond pure proton conductors, mixed proton and electronic (either p-type[17] or n-type[4]) conduction occurs in certain oxides of multivalent ions. The rich compositional space available to these classes of inorganic conductors suggests their properties can be tuned to potentially achieve even higher proton conductivities, motivating efforts
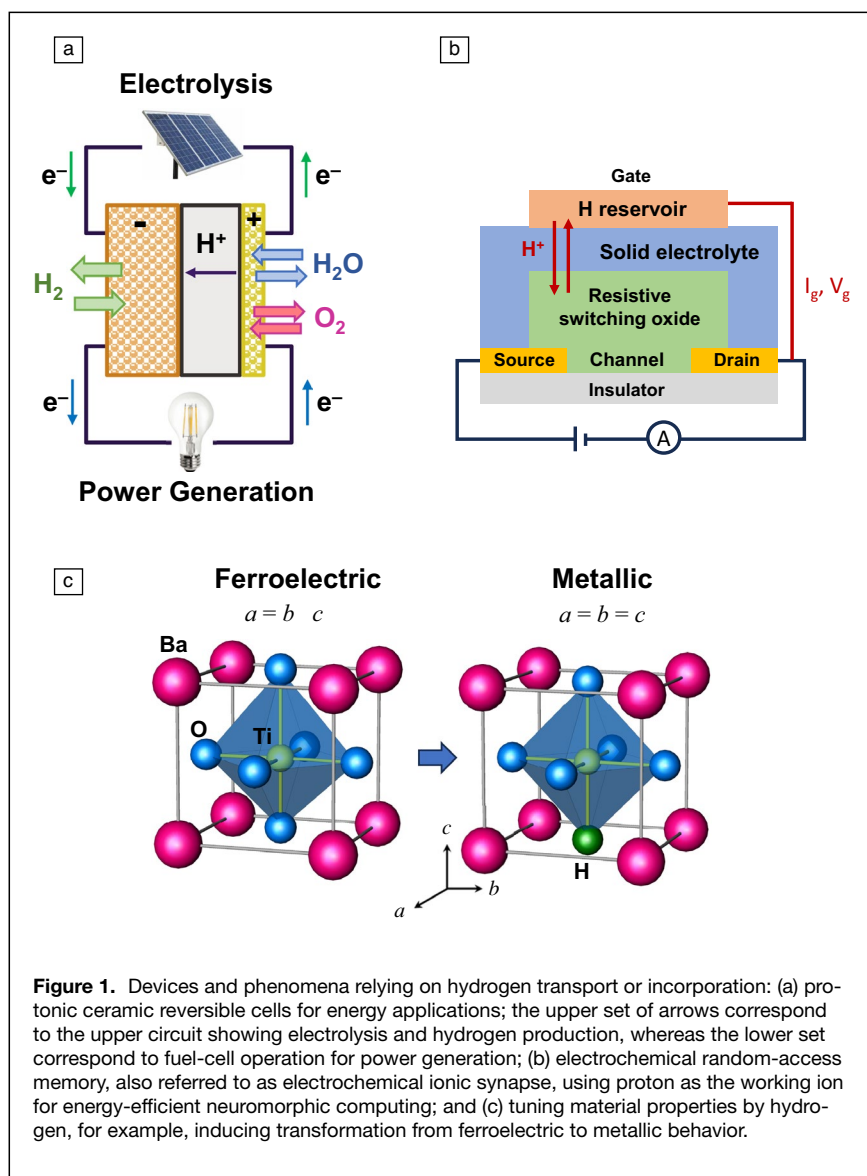

Figure 1. Devices and phenomena relying on hydrogen transport or incorporation: (a) protonic ceramic reversible cells for energy applications; the upper set of arrows correspond to the upper circuit showing electrolysis and hydrogen production, whereas the lower set correspond to fuel-cell operation for power generation; (b) electrochemical random-access memory, also referred to as electrochemical ionic synapse, using proton as the working ion for energy-efficient neuromorphic computing; and (c) tuning material properties by hydrogen, for example, inducing transformation from ferroelectric to metallic behavior.

to develop a deep understanding of the proton conduction mechanisms.

Solid acids of high proton conductivity are composed of metal cations and a network of polyanion groups (e.g., SeO_4, SO_4, PO_4) that are linked to one another solely by hydrogen bonds. At ambient temperatures, the rigid hydrogen-bonding network in such materials results in moderate proton conductivities ($\sim 10^{-5}$ S/cm).[8,18] In a subset of compounds in this class, the material undergoes a first-order transition to a state of high conductivity ($>10^{-3}$ S/cm), typically at a temperature between 100 and 300°C.[8,11,18,19] Protons migrate via proton transfer between oxygens of neighboring polyanion groups, followed by lattice rearrangement via polyanion-group rotation (see **Figure 2**a), an example of the Grotthuss mechanism. Two characteristic features of the superprotonic phase enable fast proton conduction.[8,18,20] First is the facile rotation of polyanion groups, akin to polyanion sublattice rotational melting. Second is the accompanying dynamical disorder of the hydrogen bond network.[19] The rate-limiting step may be either proton-hopping, as suggested for superprotonic $CsHSO_4$,[21] or polyanion reorientation, as suggested for superprotonic CsH_2PO_4.[21,22]

The most studied ternary metal–oxide proton conductors have the perovskite (ABO_3) structure, consisting of corner-sharing BO_6 octahedra, such as $BaZrO_3$ and $BaCeO_3$.[15,16] Protons are typically incorporated through hydration. Here, absorbed water dissociates into OH^- groups and protons, with the former filling oxygen vacancies created by doping, and the latter binding to lattice oxygens to also form OH^-.[14] The proton-hopping step in this case requires transfer between nearest neighbor oxygens, then the newly formed OH^- group rotates about the B–O–B axis of the acceptor to prevent backward shuttling to the donor (see Figure 2a).[14] Although aliovalent dopants are essential in proton incorporation by introducing vacancies, they can also limit proton mobility, either through electrostatic binding and trapping,[23] or by hardening of bending modes.[24] Other related crystal structures that have achieved promising proton conductivities are Ruddlesden–Popper[25] and brownmillerite,[26,27] respectively. Although the local geometries may differ between crystal structures, ternary oxides generally share a similar Grotthuss mechanism, involving proton-hopping and lattice rearrangement via the OH^--group rotation.[14] The former, the proton-hopping, is argued to be the rate-limiting step in ternary metal–oxide proton conductors.[8,14,28–30]
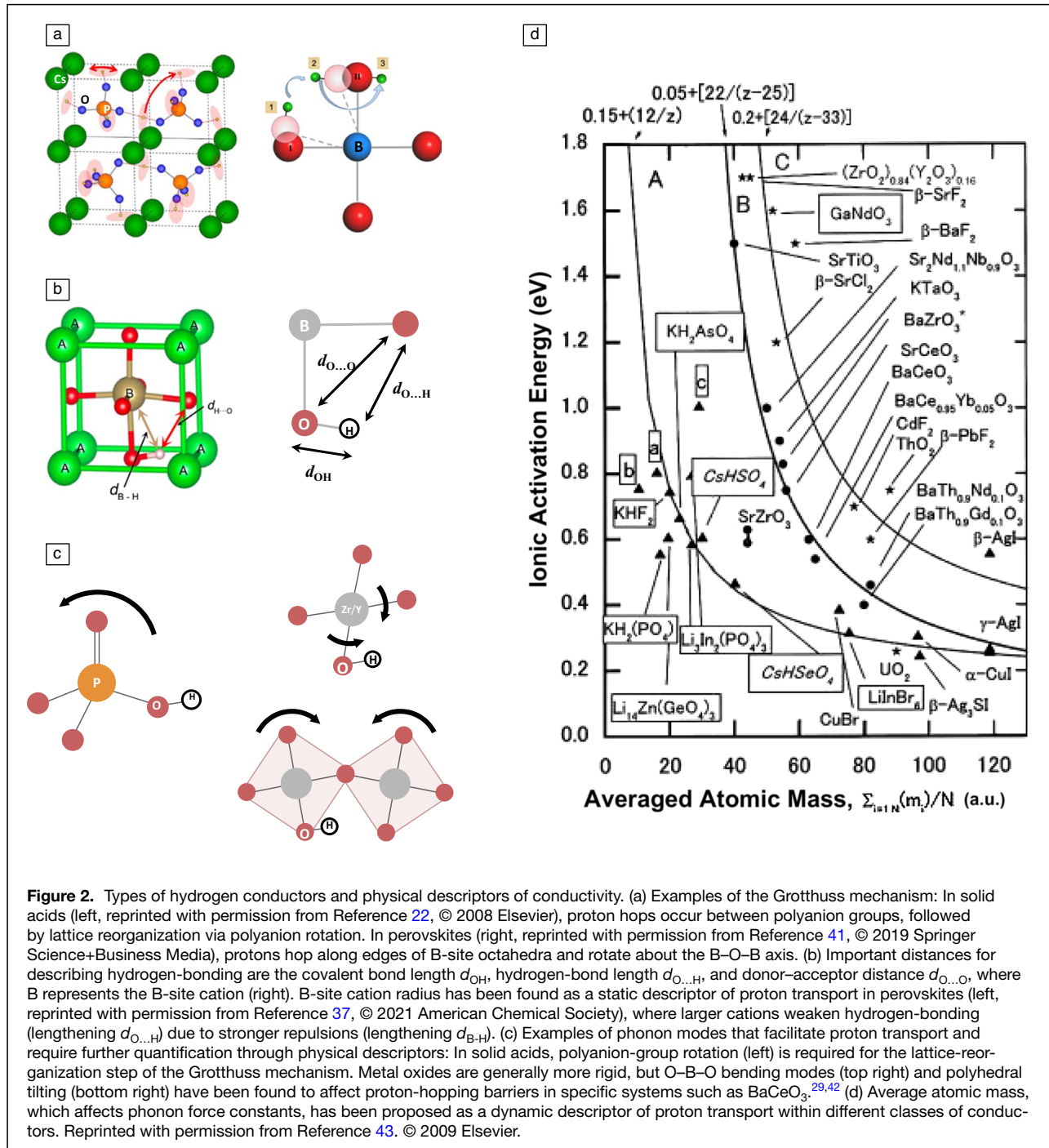
When a metal oxide contains a multivalent cation,[27,31–33] it is possible to incorporate protons without aliovalent dopants. This involves direct H incorporation (either from H_2 or H_2O), which reduces the metal and binds protons to oxygen atoms. In some cases (e.g., $BaPrO_3$[33]), the hydrogenation creates a mixed protonic–electronic conductor, whereas in others (e.g., $Sr_2Co_2O_5$[27]), hydrogenation suppresses electronic conduction, rending the material a pure proton conductor. The surprising behavior of $Sr_2Co_2O_5$ has been explained by first-principles calculations and XAS measurements, which have demonstrated

that formation of strong O–H bonds decreases covalency of neighboring O–Co bonds and thereby widens the bandgap.[27] Beyond the goal of developing advanced proton-conducting electrolytes, proton incorporation into variable valence oxides provides a means of precise control of electronic and magnetic properties.[34] The electrochemical synaptic device illustrated in Figure 1b exploits this behavior of oxides such as WO_3 and V_2O_5,[4,35] where hydrogen incorporation generates electron polarons. Such materials, with protons as the working ion, are also of interest in electrochromic[36] applications. Explicit efforts to create mixed proton and electronic conductors have been pursued by combining aliovalent doping, for oxygen vacancy generation, with transition-metal doping, for hole creation. A key example of this is $BaCo_xFe_{0.8-x}Zr_{0.1}Y_{0.1}O_{3-\delta}$, which has shown tunability with dopant concentration for the oxygen reduction reaction in protonic ceramic fuel cells.[17] In cases where multiple charged mobile species are spatially localized (i.e., polarons and protons, or oxygen vacancies and protons), further research is necessary to understand whether and how their diffusion mechanisms may be coupled, for example, through point defect binding or concerted motion.

Descriptors of lattice proton conductivity

Understanding the quantitative relations of chemical, structural, electronic, and dynamic traits of the materials to the proton conduction mechanisms is important for advancing proton conductivity. In the field, such traits are also referred to as descriptors. We believe these descriptors can guide the discovery and design of materials with high proton conductivity only if they are physically based and interpretable in their relation to the proton conduction mechanism. Criteria for good descriptors include being physically based, having a strong correlation with the steps of the conduction mechanism, simplicity, ease of estimation, and generalizability. Good descriptors can both enhance our understanding of proton migration and enable interpretable, high-throughput screening and discovery of fast conductors within these materials classes.

We can categorize the descriptors of proton conduction to represent the static traits of a material, characterized by atomic structure, bond lengths, chemistry, electronic structure, as well the lattice dynamic traits, characterized by phonon modes and bond topology (Figure 2b). Given the prominence of the Grotthuss mechanism (Figure 2c) in inorganic solids, it is important to identify physically based descriptors both for the proton-hopping step and for the lattice reorganization step. Several static descriptors of proton-hopping have been explored in the field. Since strong hydrogen-bonding leads to facile proton transfer, the energy barrier of this step has been correlated with hydrogen-bond length, $d_{O \cdots H}$, in double perovskites,[37] ternary oxides,[38] and sulfate solid acids.[8] Based on a high-throughput screening of double perovskites, Islam et al.[37] found that smaller B-site cations with lower oxidation states lead to lower proton-hopping barriers, arguing that larger B-site cations lengthen hydrogen-bond lengths by

Figure 2. Types of hydrogen conductors and physical descriptors of conductivity. (a) Examples of the Grotthuss mechanism: In solid acids (left, reprinted with permission from Reference 22, © 2008 Elsevier), proton hops occur between polyanion groups, followed by lattice reorganization via polyanion rotation. In perovskites (right, reprinted with permission from Reference 41, © 2019 Springer Science+Business Media), protons hop along edges of B-site octahedra and rotate about the B–O–B axis. (b) Important distances for describing hydrogen-bonding are the covalent bond length d_{OH}, hydrogen-bond length $d_{O...H}$, and donor–acceptor distance $d_{O...O}$, where B represents the B-site cation (right). B-site cation radius has been found as a static descriptor of proton transport in perovskites (left, reprinted with permission from Reference 37, © 2021 American Chemical Society), where larger cations weaken hydrogen-bonding (lengthening $d_{O...H}$) due to stronger repulsions (lengthening d_{B-H}). (c) Examples of phonon modes that facilitate proton transport and require further quantification through physical descriptors: In solid acids, polyanion-group rotation (left) is required for the lattice-reorganization step of the Grotthuss mechanism. Metal oxides are generally more rigid, but O–B–O bending modes (top right) and polyhedral tilting (bottom right) have been found to affect proton-hopping barriers in specific systems such as BaCeO$_3$.[29,42] (d) Average atomic mass, which affects phonon force constants, has been proposed as a dynamic descriptor of proton transport within different classes of conductors. Reprinted with permission from Reference 43. © 2009 Elsevier.

repelling protons (Figure 2b). In a broader, high-throughput study of ternary oxides using first principles, Islam et al.[38] found that the presence of connected octahedra correlates with lower proton-hopping activation energy, proposing that higher coordination leads to shorter hydrogen-bond lengths. Bork et al.[28] argued that hydrogen-bond strength imposes a tradeoff between energy barrier and attempt frequency, since they found a volcano relationship between O–H bond strength and proton transport frequency.

To understand proton conduction at larger length scales, beyond the local hopping step, others have studied the topology of migration pathways. Draber et al. proposed that Y-dopants in BaZrO$_3$ form trapping zones, within which protons can hop more easily than in pure Zr environments, such that percolating paths of dopants with overlapping trapping zones can facilitate long-range proton transport.[39,40] This stands in contrast to the impact of isolated trap sites that occur at lower dopant concentrations and

can frustrate proton transport.[23] Further study of proton-site topology may be fruitful for understanding long-range conduction, particularly in systems with possible cooperative mechanisms of proton transport or in materials such as solid acids with extended hydrogen-bonded networks.

Finding generalizable, dynamic descriptors of proton conductivity remains an open area of research. This is an important direction because lattice rearrangement is an important step in proton conduction, but it is more challenging to quantify compared to the static descriptors. Phonon-based descriptors, such as projected band centers and force constants, have been found to correlate to diffusivities of O^{2-} [44] and Li^+ [45] in inorganic solids, such that the softer the phonon modes, the faster the mobility of the ion. Studies of specific crystal structures have demonstrated that lattice dynamics play a role also in proton conductivity.[42,43,46] This connection is clearest in solid acids, where reorientation of polyanion groups is necessary to transport the proton away from the donor site, and proton conduction is high only once the polyanion groups become rotationally disordered.[8,11] The ease of polyanion rotation must be encoded in certain phonon modes and frequencies. Kreuer[8] noted that sulfate solid acids with high conductivity have high Debye–Waller factors of the central sulfur atom and large radii of the counter-cations, hypothesizing that polyanion groups separated by larger cations have weaker hydrogen-bonding to enable easier group rotation. In perovskite and other ternary oxide proton conductors, the structure is more rigid than in solid acids, and the metal–oxygen polyhedra are not expected to rotate. Generally, the rate-limiting step is thought to be proton-hopping.[8,14,28–30] However, lattice dynamics are still likely to be important in this class of conductors since distances between acceptor and donor atoms can be affected by vibrational motion at finite temperatures. For example, using *ab initio* molecular dynamics (AIMD)[47] and energy-barrier calculations,[46] Munch et al. showed by atomistic simulations that decreasing donor–acceptor distance $d_{O \cdots O}$ induced by thermal fluctuation is essential for enabling proton-hopping in perovskites $BaTiO_3$, $BaZrO_3$, and $BaCeO_3$. Phonons such as the O–B–O bending mode shorten $d_{O \cdots O}$ and increase the overlap between the acceptor and donor electron clouds, which may help to lower the energy barrier of proton-hopping. Gomez et al.[29] also studied a set of four perovskites to understand how octahedral tilting affects proton-binding sites and transition pathways. Based on AIMD trajectories of hydrated 12.5% Y-doped $BaZrO_3$, Torayev et al.[24] studied how these distortions are induced by doping and thermal vibration, as well as the effect on proton transport mechanisms. One of the broadest studies of lattice dynamics and proton conduction was performed by Wakamura et al.[43,48] Arguing that average atomic mass, unit-cell volume, and optical dielectric constant all affect force constants, they correlated these phonon-adjacent descriptors with effective energy barriers and transition temperatures within the materials classes of perovskites and solid acids (see Figure 2d). These findings confirm the importance of lattice dynamics in different classes of proton

conductors. Next, developing quantitative descriptors that can identify specific phonon modes facilitating proton transport, relating proton diffusivities directly to phonon calculations, and generalizing to broader classes of materials is needed in the field.

Hydride ion conductors

A hydride ion in solid-state matter consists of a proton with two loosely bound electrons and holds promise as a fast charge carrier due to its small mass and high polarizability (or anion softness). Verbraeken et al. synthesized BaH_2 as the first hydride ion conductor,[49] and the material has achieved ionic conductivities up to 0.3 S/cm at 600°C.[50] A concerted migration mechanism has been proposed,[50] driven by geometric frustration. Geometric frustration is a form of configurational disorder that occurs when competing structural constraints prevent energy minimization. At the superionic transition temperature near 500°C, BaH_2 transforms from a distorted HCP structure to a higher-symmetry hexagonal structure, which is overconstrained. In this high-temperature phase, frustrated D1 hydride ions oscillate between competing sites and can trigger concerted migration of neighboring anions due to Coulombic repulsions.

Oxygen-substituted lanthanum hydrides with densely packed H have exhibited impressive conductivities of up to 1 mS/cm at room temperature.[51,52] These systems have a face-centered-cubic (fcc) structure, where a rhombic dodecahedron of hydride ions surrounds each lanthanum site and oxygen substitution is necessary to suppress electronic conduction. Although the doping is beneficial for lowering electronic conductivity, trapping of hydride ions near oxygen dopants has been observed in molecular dynamics simulations. Fukui et al. argue that a neighboring dopant increases the charge on the La ion and strengthens its association energy with nearby H^-.[52] For mobile ions far from dopants, a cooperative transport mechanism has been suggested where H^- in octahedral sites repel H^- in nearby tetrahedral sites.[51] This cooperative mechanism may be enabled by the soft, dense H^- sublattice, where the small mass and high polarizability lead to high vibrational amplitudes and anharmonicity.[52] Because dopant sites cause trapping, oxygen concentration must be low enough to allow percolating domains of mobile ions that can undergo concerted migration.[51] In hydride-substituted perovskite oxides, such as $BaTiO_{3-x}H_x$, charge transport is dominated by electronic conductivity,[53,54] but exchange between H^- and $O^=$ and hence significant H^- mobility is inherently implied by the preparation routes, which typically involve reaction of the oxide with a metal hydride such as CaH_2. Direct measurements of the H^- diffusivity reveal that hydride transport properties are dependent on the availability of vacant anion sites.[55,56]

Finally, nitrohydrides such as Ca_2NH are of particular interest as catalysts for ammonia synthesis.[57] Ca_2NH has a rock-salt-like structure with two phases: a disordered phase with low ionic conductivity, and a higher-symmetry phase that has shown high diffusivities of 1.6×10^{-5} cm^2/s at 600°C.[57]

However, the overall conductivity of 0.08 S/cm is much lower than that of BaH_2 at the same temperature. This is believed to result from the vacancy-mediated diffusion of H^- in Ca_2NH[57] in contrast to the concerted migration mechanism of BaH_2. Given the observed behavior and proposed mechanisms for Ca_2NH, BaH_2, and doped LaH_3, it is possible that higher hydrogen concentrations (dense, extended H^- sublattice) cause concerted transport mechanisms to dominate and lead to higher conductivities. These observations suggest that exploration into soft phonon modes which participate in hydride ion migration could be fruitful.[52]

Interfacial proton transport

The kinetics of proton transport across and even along solid–solid interfaces plays a crucial role in the performance of both electrochemical energy and information devices. In electrochemical systems, electrolytes are typically polycrystalline, and the grain boundaries of such materials, which generally impede proton motion, have been the subject of extensive investigation.[58,59] Proton transport across electrolyte–electrode interfaces has garnered much less attention, but has recently emerged as a potential bottleneck in advancing device performance metrics.[1,60–62] In electrochemical synaptic devices,[5,6] in which the electrolyte is exceptionally thin, the critical parameters of switching voltage and speed are directly dependent on the kinetics of H transfer across electrolyte | channel (intercalant) interface, and careful studies of such interfaces are just beginning to be reported in the literature. By nature of its occurrence in series with lattice transport, transport across interfaces is detected only if it is an impediment to the overall process. In contrast, proton transport along interfaces, which occurs in parallel with lattice transport, offers opportunities for enhancing macroscopically observed properties. This is particularly true of materials with low bulk or lattice conductivity.[41,63]

In this section, we provide an overview of proton transport both across and along solid-state interfaces, as broadly illustrated in **Figure 3**. To date, the influence of such interfaces on hydride ion transport has not been evaluated and accordingly is not treated here.

Transport across solid-state interfaces

Solid–solid interfaces in electrochemical systems include both grain boundaries and heterointerfaces between dissimilar materials. As widely appreciated, the crystallographic disruption inherent to grain boundaries often induces changes in chemical composition and enhances impurity concentrations relative to the bulk.[64] In ionic materials, the grain-boundary core may furthermore favor the local formation of certain charged ionic defects (e.g., oxygen vacancies), which is then accompanied by adjacent charge-compensating space charge regions.[59,65,66] Heterogeneous interfaces may also exhibit space charge regions with carrier enhancement or depletion, depending again on the nature of the core of the interface. Space charge models (e.g., Mott–Schottky, Gouy–Chapman)
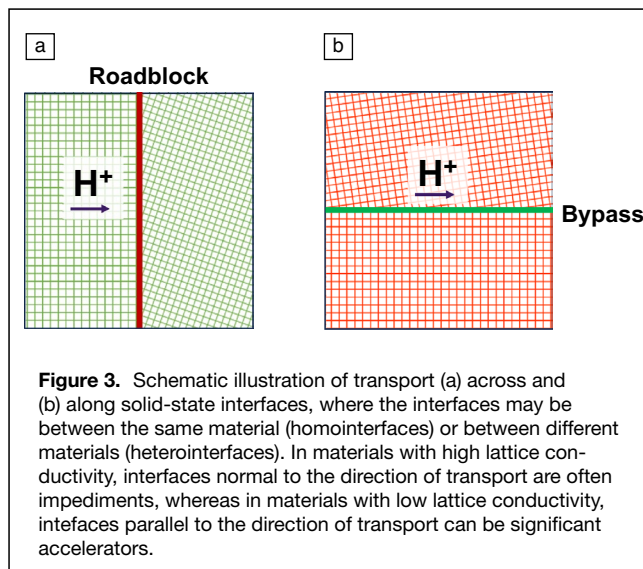

Figure 3. Schematic illustration of transport (a) across and (b) along solid-state interfaces, where the interfaces may be between the same material (homointerfaces) or between different materials (heterointerfaces). In materials with high lattice conductivity, interfaces normal to the direction of transport are often impediments, whereas in materials with low lattice conductivity, intefaces parallel to the direction of transport can be significant accelerators.

can be used to describe carrier and mobile defect concentration profiles in the adjacent zones when concentrations are dilute, whereas the Poisson–Cahn theory can be used to describe systems beyond the dilute limit.[67] The defect concentrations delineating these regimes between noninteracting and interacting defects are material specific, but a 1% concentration can typically be safely treated in the dilute limit framework, and even systems with defect concentrations as high as 20% can be adequately described.

Grain boundaries

Grain boundaries in oxide lattice proton conductors typically exhibit blocking effects. This may be caused by the depletion of protons in space-charge zones, the formation of lower conductivity or even insulating secondary phases, or a decrease in mobility due to disruption of the structure.[59] In contrast, in superprotonic solid acid conductors, a detrimental impact of grain boundaries has never been reported. Instead, retention of surface adsorbed species can enhance the overall conductivity.[68] Other classes of proton conductors rely entirely on favorable surface transport resulting from adsorption and absorption of water layers at pores and grain boundaries[69,70] as discussed below in the context of transport along internal surfaces. Thus, grain boundaries can influence proton transport either positively or negatively, depending on the host material.

Disentangling the competing roles of carrier depletion in space-charge zones and mobility decline across crystallographically distorted interfacial regions on proton transport remains a scientific challenge. Moreover, it is unlikely these effects occur in isolation. Nevertheless, notable progress in characterizing and understanding these phenomena has been made in recent years. It is now relatively well established, for example, that the macroscopic impedance of grain boundaries in $BaZrO_3$ (BZO) is more severe than in $BaCeO_3$ (BCO). Lindman et al. suggest, on the basis of density functional theory (DFT) calculations of

undoped compositions, that this is a result of preferential segregation of protons to the grain boundaries of BZO, which is then reflected in a higher space-charge potential.[71] In Y-doped BZO, an increase in dopant accumulation in the grain boundaries with doping level has been observed, and the accompanying decrease in specific grain-boundary resistivity has been attributed to dopant screening of the grain-boundary charge,[72] lending credence to the hypothesis that high grain-boundary impedance in BZO is due to space-charge effects.[73] On the other hand, an in-depth analysis revealing disagreements between the space-charge model and experimental data has been used to suggest that the proton mobility across the grain-boundary zone in $BaZrO_3$ is significantly diminished.[74] Furthermore, comparisons of the specific grain-boundary impedances of doped BZO[75] and doped BCO[58] suggest similar properties, with the macroscopically observed high impedance in doped BZO then arising from the typically smaller grains and hence higher number density of grain boundaries in the zirconate.

While the origin of high impedance for proton transport across grain boundaries remains unresolved, its negative impact on macroscopic conductivity is widely recognized. Accordingly, significant effort has been directed to both increasing grain size, particularly in doped BZO, and decreasing the specific grain-boundary impedance. Transition-metal additives NiO and ZnO serve to enhance sinterability of doped BZO, allowing for significant grain growth and densification at moderate sintering temperatures (1300–1400°C).[76–78] However, both have negative impacts on transport properties. NiO lowers the effective acceptor concentration in the bulk of Y- and Sc-doped BZO, decreasing proton uptake and thus proton conductivity,[79] although the Ni itself likely remains concentrated in the grain-boundary regions.[80] Similar to NiO, ZnO accumulates in the grain boundaries of the host perovskite. In $BaCe_{0.35}Zr_{0.5}Y_{0.15}O_{3-\delta}$ (BCZY), the accumulation is correlated with a decrease in the specific grain-boundary conductivity, in turn, attributed to an increase in the grain-boundary potential.[81] The additive $LiNO_3$ has been suggested as a fugitive sintering aid for Y-doped BZO, which provides the benefits of enhanced sintering, but due to its volatility, $LiNO_3$ does not remain in the structure and hence has no detrimental impact on conductivity.[82]

Heterointerfaces

Despite the prevalence of heterointerfaces in solid-state electrochemical devices, proton transport across electrode–electrolyte interfaces has rarely been characterized. To some extent, this implies that the impedance of such interfaces is low. Nevertheless, their role in device functionality cannot be entirely ignored. In high-performance fuel cells and electrolyzers based on perovskite proton conductors such as $Ba(Zr_{0.4}Ce_{0.4}Y_{0.1}Yb_{0.1})O_3$[1,60] and $Ba(Zr_{0.1}Ce_{0.7}Y_{0.1}Yb_{0.1})O_3$,[61,62] residual resistance terms, those that cannot be directly attributed to the electrolyte or either electrode, are significant contributors to the cell overpotential. In such devices, the thin electrolyte is supported on a thick

electrode, often formed as a composite of the electrolyte material and Ni metal, which serves as the negative electrode (negatrode) in both fuel-cell and electrolyzer configurations. The positive electrode (positrode), almost universally a transition-metal-bearing oxide, is applied as a final step atop the bilayer structure. Treatments of the electrolyte surface that enhance the adhesion between the electrolyte and the positrode material have proven effective in decreasing the residual resistance, implicating this interface as the culprit. Such treatments include deposition of a thin dense layer of the oxygen electrode material by pulsed laser deposition,[60] acid etching of the electrolyte surface,[61] and mechanical polishing of the electrolyte surface.[62] While all methods likely improve the area of contact, mechanical polishing is shown to further remove a Ba-deficient layer formed during high-temperature sintering, plausibly eliminating an additional source of high impedance.

In contrast to proton transport across electrolyte|electrode interfaces in high-temperature protonic ceramic fuel cells and electrolytes, which nominally leaves the oxidation state of the electrode material unperturbed, H^+ transport across the electrolyte|channel material interface in electrochemical synaptic devices inherently requires a change in oxidation state of the channel material for device functionality. Here, (de)intercalation of H^+ in the channel (Figure 1b) modulates its electronic conductivity via both electronic charge compensation and modified electronic carrier mobility.[4] In ultrathin devices subject therefore to high electric fields, proton transfer through the electrolyte layer is rapid, and the heterointerface becomes the kinetic bottleneck.[6] Efficient proton transfer across the electrolyte|channel interface (coupled with electronic carrier injection/removal from the outer circuit) is necessary to ensure a low overpotential, fast conductance modulation, and fast conductance settling in the channel.[5] However, in emerging inorganic devices with a WO_3 channel interfacing a phosphosilicate glass (PSG) electrolyte, the interfacial H transfer kinetics are not yet optimized (the target interfacial exchange current density is on the order of $j_0 = 0.1–1$ A cm^{-2} for fast potentiation).[5] Particularly for long pulse lengths, slow diffusivity of H in H_yWO_3 can lead to a H buildup at the heterointerface during H insertion that can generate catastrophic H_2 bubble formation.[6] Engineering faster H diffusivity in the channel side of the heterointerface would ameliorate this degradation pathway. Alternatively, in devices where H transfer across the interface is much less facile (e.g., H-conducting HfO_2 electrolytes interfacing In–Ga–Zn–O channels), the channel conductance may be modulated at low voltages by electric double-layer formation as H^+ accumulates on the electrolyte side of the interface, rather than by full H^+ intercalation into the channel. In this case, poor performance has been attributed to traps (presumably electronic trap states) at the electrolyte|channel heterointerface, namely interfacial oxygen vacancies. It was found that oxygen plasma treatment effectively reduces the interface trap density, which then translates into enhanced linearity and symmetry of the synaptic

weight (conductance) change, with an increased on/off current ratio. Postannealing and electric-field application may also modulate the interface trap density, as has been more widely studied in the context of H trapping at Si|SiO_2 interfaces.[83] The sparse literature on such interfaces reflects the infancy of the electrochemical synaptic device approach and suggests rich opportunities for unraveling the possible influence of space-charge effects, impurity segregation, elemental interdiffusion, and strain at the heterointerface on local proton mobility.

Transport along internal surfaces

In contrast to transport across solid-state interfaces, proton transport along internal surfaces often occurs at an enhanced rate relative to bulk transport. In materials with high lattice proton conductivity, this enhanced transport may not be detected as a consequence of the small volume occupied by internal surfaces. For those with poor lattice conductivity, however, surface transport may be the predominant mechanism of proton conduction.[69,70,84–86] Examples here include stacked two-dimensional materials, several binary metal oxides, and layered clays. Such behavior is particularly true of fluorite-structured oxides. When formed as nanocrystalline compacts, many in this class display significant grain-boundary conductivity generally attributed to protons resulting from the adsorption of water within the loosely packed grain-boundary regions.[69,84,85,87] Taking surface transport to the extreme, precise design of interfacial properties by adjoining heterogeneous materials holds promise as a strategy for creating superhighways for proton transport, and we discuss both porous and architected composites next.

Nanoporosity and surface conduction of protons

Among materials with conductivity dominated by transport along internal surfaces, fluorite-structured oxides, including Y-stabilized ZrO_2 (YSZ)[69,70,87] and CeO_2 (with and without dopants),[88,89] have received significant attention. The importance of internal surfaces has been demonstrated by the dependence of the conductivity on pore size, humidity, and temperature. In contrast to conventional ion conductors, the proton conductivity decreases with increasing temperature above ambient due to desorption of H_2O from the interfacial regions. The connectivity of the porosity has also proven critical in modulating proton conductivity, as demonstrated by improved performance in different systems after sintering-free compaction due to nanoconfinement of adsorbed water layers.[90] Although disorder inhibits precise understanding of glass microstructure, pore size can be indirectly controlled through fabrication conditions and estimated using thermogravimetry and gas sorption. For example, indirect controls used for hydrogel and thin-film P-doped a-SiO_2 have been additives[91] and deposition pressure,[92] respectively. In both cases, smaller pores led to improved proton conduction under low humidity, attributed to better water retention and nanoconfinement. Similarly, acid-in-clay electrolyte[93] has exhibited fast proton conduction due to a hypothesized

packed-acid mechanism, where overlap in solvation shells of H_3O^+ weakens local H-bonding and enables facile H_3O^+ rotation for the second Grotthuss step.

Depending on the phase of adsorbed water, either the Grotthuss (ice-like) or vehicle (liquid-like) mechanism can dominate, where the relative contributions can be measured by the H/D isotope effect. A layered structure of adsorbed water has been established, based on vanishing H/D isotope effect at higher humidities,[94] along with thermogravimetric analysis, IR spectroscopy, and NMR.[90] The first hydration layer consists of chemisorbed water, which dissociates to passivate dangling bonds at the solid surface. At moderate humidities, the first layer of physisorbed water forms with rigid, ice-like structure, followed by subsequent physisorbed layers with liquid-like structure at high humidity.[95]

Heterointerfaces

Proton conductivity along heterointerfaces is an emerging area of study, where transport in principle could be enhanced or hindered by the effects of elastic or plastic strain, crystallographic distortions, and point defect redistribution (e.g., interdiffusion, segregation, and space-charge regions)—in other words, by coupled structural and electrostatic factors.[96,97] A small lattice mismatch across coherent heterointerfaces can give rise to elastic strain, influencing the activation enthalpy of charge-carrier migration as well as point defect formation energies. In the case of larger lattice mismatches, dislocations may form with potential to enhance proton conductivity.[97] For example, in the case of $BaZr_{0.8}Y_{0.2}O_3$ (BZY) films on $NdGaO_3$ (NGO) with ~10% lattice parameter difference, a network of misfit dislocations forms. The apparent enhanced in-plane proton transport (parallel to the heterointerface) has been variably attributed to local cation nonstoichiometry, excess oxygen vacancies distributed along the dislocation cores enabling proton incorporation, and distortions of oxygen octahedra in strained regions between dislocations.[98]

A particular application of leveraging H transport along heterointerfaces is in composite electrolytes. For example, $BaCo_{0.4}Fe_{0.4}Zr_{0.1}Y_{0.1}O_{3-\delta}$|ZnO was developed to be a composite electrolyte by suppressing the electronic conduction via the p–n junction structure, maintaining good $H+$/O^{2-} conductivity along the interfaces.[99] Similarly, high proton conductivity was found in a composite CeO_2|$BaZr_{0.8}Y_{0.2}O_{3-\delta}$ electrolyte.[100] In both cases, fast interfacial ionic transport was attributed to the built-in electric field (space-charge effect) at the interface. One way to prepare composites with aligned interfaces in the direction of transport in devices is to grow vertically aligned nanocomposites (VANs). While VANs have not yet been applied in the context of H transfer, they have been occasionally developed for oxide ion conductors, for example, to increase the triple phase boundary density and thus the active sites for electrochemical reactions in electrodes supporting oxygen exchange at the solid–gas interface and to modify oxide ion transport along the transport direction

in electrolytes. For instance, a VAN electrolyte composed of $(Ce_{0.9}Gd_{0.1}O_{1.95})_{0.5}|(Zr_{0.92}Y_{0.08}O_{1.96})_{0.5}$ (GDC/YSZ) reportedly provided superior out-of-plane oxide ion conductivity, which may be caused by the lattice strain at the interface and the fast ion transport path along the vertical heterointerfaces.[101]

External drivers to influence hydrogen transport

Beyond the composition and structure that one obtains upon synthesis of a compound, material properties, including proton or hydride ion conduction, can be modulated by external drivers. These external drivers, such as mechanical strain, electric field, and light, can alter the energy landscape such that both the stability and the mobility of the ion become different from those in the as-synthesized equilibrium state.

Investigation into the effect of mechanical strain on proton conductivity has been motivated by analogous studies on other ionic conductors. For example, oxide ion conductivity has been observed to increase under biaxial tension, attributed to a decrease in the oxygen metal bond strengths.[102–106] Similarly, lithium-ion conductivity has demonstrated tunability through anisotropic biaxial strain.[107,108] It is generally accepted, largely on the basis of studies of epitaxially strained thin films, that proton conductivity in perovskite oxides decreases under compression and increases under biaxial tension.[109–111] However, the precise mechanisms underlying these effects remain a subject of ongoing debate. Fluri et al.[110] applied AIMD to $BaZrO_3$, with and without dopants, and argue that tension weakens interaction between dopants and nearby trapped protons, whereas Hyodo et al.[111] claim that strain primarily increases proton mobility far from dopants by softening relevant phonon modes, without significant effects on near-dopant trapping. Under high compressive stress, the O–B–O bending and especially the O–B stretching modes of Y-doped $BaZrO_3$ harden.[112] This suggests a third possibility for the impact of tensile strain: that it may act in reverse of compression to soften phonons and thereby facilitate proton transport. Further investigation is required to establish how strain affects proton positions in the lattice and relevant phonon frequencies, and ultimately what the dominant mechanisms of the strain effect are. Exploring strain effects in other proton conductors beyond perovskites can also provide insight into the generalizability of these findings.

Relatively few studies of the impact of extreme electric field on proton transport have been reported, and the opportunities for achieving nonclassical effects appear rich. A tantalizing example emerges from the behavior of phosphosilicate glass. Typically, nanoporous oxides exhibit proton conductivity only under high humidity via the surface conduction mechanisms previously discussed.[91,92] However, Onen et al.[6] fabricated protonic electrochemical synaptic devices (Figure 1b) with thin-film, phosphosilicate glass (PSG) electrolytes, which achieved ultrafast switching (ns regime) despite lack of controlled humidity. This speed was enabled by external fields as strong as 1 V/nm, which

were possible due to the high dielectric strength of PSG under relatively dry conditions. Under classical theory, high electric field can accelerate ionic motion resulting in superlinear response.[113] However, it is unclear whether the observed phenomena can be fully explained in this manner as strong electric fields may induce nonclassical effects, such as polarization of the covalent O–H bonds and softening of the lattice, leading to changes in proton-hopping barriers. For example, earlier work found that, even in nonpolar compounds, external electric field lowers the formation energy of oxygen vacancies due to polarization of electrons in the vacancy, as well as softening of phonons induced by the defect formation.[114] Further research is needed for resolving the mechanisms by which proton transport is affected under strong electric fields, relevant especially to thin-film devices where very high electric fields exist.

Light as an external stimulus has also shown promise to tune ionic transport, but has not yet been exploited for proton or hydride ion conductors. An interesting and motivating example was from oxide ion conductors. Defferriere et al. demonstrated that above-bandgap illumination can increase oxide ion conductivity in Gd-doped ceria by modifying space-charge regions adjacent to grain boundaries.[115] Because space-charge effects are also likely contributors in blocking proton conduction across the grain boundaries of hydrated perovskites (as previously discussed), it may be possible to leverage an optical approach similar to that of Defferriere et al. to enhance total proton conductivity in perovskites.

Advances in methods to probe the nature of H in solids

To address the outstanding scientific questions above and realize proton-enabled technologies for energy conversion, energy storage, and energy-efficient computing, it is vital to accurately characterize the atomic structure, dynamics, and diffusion of hydrogen within solid oxides and functioning heterostructures and devices. With its low atomic weight and size, hydrogen is very difficult to directly observe in materials.[116] Because hydrogen has no electrons in the k-shell, energy-dispersive spectroscopy (EDS) techniques cannot be applied for its detection. Depending on the technique, characterization is also made more challenging by low concentrations within the host solid and poor contrast of hydrogen relative to other atoms being probed. Modern advances in instrumentation techniques and modeling are enabling a new frontier in the characterization of the nature and behavior of hydrogen with electron microscopy,[117] neutron scattering,[118] scanning probe microscopy,[119] nuclear magnetic resonance (NMR) spectroscopy,[23,120,121] and time-of-flight secondary ion mass spectrometry (ToF–SIMS),[55,122] attaining detection of extremely low concentrations. These methods extend our understanding of hydrogen in materials beyond the insights possible from more accessible methods such as gravimetric analysis, thermal desorption spectroscopy, and electrochemical impedance spectroscopy, typically employed for characterizing hydrogen

sorption and desorption from surfaces and transport in the bulk.[116]

Resolution of hydrogen environment

Knowledge of the location, the local environment, and the oxidation state of hydrogen in a solid material is an essential starting point to understanding its impact on material properties. Yet, hydrogen is particularly difficult to detect by many conventional methods. In the following, we highlight recent compelling advances in characterization methodologies that have resolved open questions in the field. The power of neutron scattering and NMR spectroscopy methods in characterizing hydrogen in solid-state matter is perhaps widely appreciated. Recent advances in x-ray and particularly electron methods mean that these tools are gaining significance for the study of hydrogen.

Diffraction and microscopy methods

Because of the negligible scattering cross section of hydrogen with x-rays and electrons, diffraction studies using these probes have typically been used to observe the influence of hydrogen uptake or removal on the host structure rather than directly detecting the hydrogen itself. For example, x-ray diffraction has been employed to detect structural transitions induced in $BaTiO_3$ due to hydride incorporation.[53] In the case of electron diffraction, dynamical scattering has long prevented the acquisition of Bragg intensities for structure determination, limiting observations to qualitative analysis.[123] In recent years, improved detectors in combination with proper control of crystal rotation have reduced dynamical scattering,[124] with implications for assessing crystallographic influences of hydrogen in host materials even when only very small crystals are available. Similarly, electron microscopy imaging of hydrogen had been essentially impossible prior to recent breakthroughs in integrated differential phase contrast (iDPC)

in conjunction with scanning transmission electron microscopy (STEM). In a remarkable demonstration of the power of this approach, columns of H atoms have been imaged in γ-TiH (**Figure 4**a) and established iDPC-STEM as a method to image H next to heavier atoms.[117]

Neutron-scattering methods have long been employed to study the nature of hydrogen in solids, spanning investigations of hydrides, porous materials (such as MOFs), carbon media (e.g., graphite and nanotubes), zeolites, metal oxides, and ice clathrates.[118] Neutrons are highly sensitive to elements such as hydrogen and oxygen, and because they are scattered by the nucleus of an atom, they are sensitive to isotopic substitution.[125] Because ^1H has a large incoherent cross section that interferes with elastic neutron scattering, D is often used as a surrogate to determine average static positions of hydrogen in a wide range of solids using neutron diffraction, including in oxides.[118,126,127] *In situ* neutron powder diffraction at variable temperature allows for the direct determination of hydrogen positions in a crystalline structure, and assessment of H dynamics with heating. Advanced analysis methods such as H/D exchange, maximum entropy methods, Fourier difference maps, and symmetry mode analysis applied to *in situ* measurements of oxides with H and D substitution make neutron diffraction a powerful tool for obtaining the structure of hydrogen in solids and even for gaining insights into diffusion pathways.[127,128] Figure 4b highlights the benefits of such an approach where the structural change in a deuterated hydroxyl (OD^-) anion, visualized with Fourier difference maps, can be measured through phase transitions over variable temperature using neutron diffraction.[127]

Complementary to average structure studies, local atomic structure can be analyzed from real-space pair distribution functions (PDFs), obtained from the Fourier transform of neutron total scattering data. PDF analysis has been used to characterize the locations and bonding of D/H in
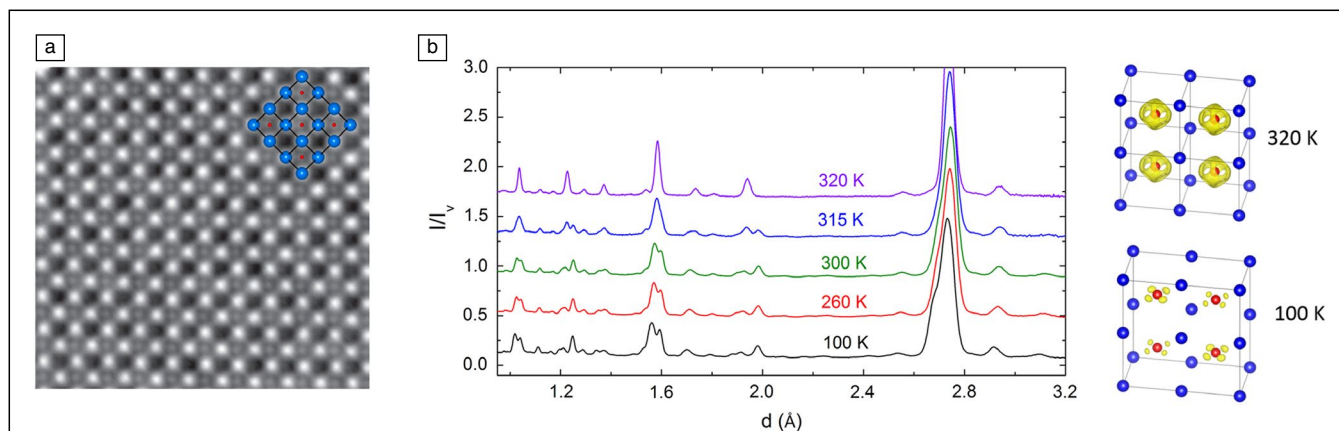

Figure 4. Detection of hydrogen in the solid state: (a) integrated differential phase contrast electron microscopy of γ-TiH utilizes phase contrast to image H positions in the fcc Ti, matching models. In the γ-TiH model inset in the upper right corner, blue indicates Ti and red indicates H sites. Reprinted with permission from Reference 117. © 2020 AAAS. (b) Fourier difference maps from *in situ* neutron diffraction reveal D sites (illustrated in yellow) in Li_2ODCl, showing a greater distribution of D around O as temperature increases. Generated from data collected in Reference 127.

amorphous and disordered material components, including in surface hydroxyls, in interlayer water species, within ligands of nanostructured materials,[129–131] as well as in bulk oxides.[131,132] For example, total scattering techniques with PDF analysis have been used to locate H/D that are occluded on molecules (such as CH_4, BH_4, and NH_2)[133] within solids. This technique reveals local structure that is often hidden (averaged out) in long-range crystallographic analysis, such as the orientation of H/D-bearing molecules in real space or the influence of disordered intermolecular and local guest–host interactions.[134–136]

Nuclear magnetic resonance spectroscopy

Similar to neutron-based techniques, NMR spectroscopy is particularly well suited to resolving the nature and local environment of hydrogen in solids. The high gyromagnetic ratio (γ) and natural abundance of ^1H imply high sensitivity in NMR detection, and the isotope sensitivity, with ^2H (deuterium) being a quadrupolar nucleus as opposed to ^1H, offers additional characterization opportunities. For the study of solid-state materials, experiments are typically performed using a magic angle spinning (MAS) method to minimize the effects of local anisotropy and achieve high spectral resolution. The positions of the resonances in the resulting spectra, noted as chemical shifts relative to some reference material, reflect the electron density surrounding the hydrogen nucleus. While there is overlap in the ranges at which these peaks occur (**Figure 5**a),[137–139] the measured positions can assist in differentiating the species.

Beyond chemical identity, information about the nearest neighbor environment can be obtained from correlation NMR experiments (Figure 5b). In materials with fast hydrogen motion (typical of high ionic conductivity), the through-space

dipolar-coupling interactions are weak, leaving through-bond J-coupling as the primary mechanism of atomic correlations. While multidimensional homonuclear or heteronuclear correlation NMR experiments provide exquisite detail regarding local environment[140] (with examples given next), even one-dimensional experiments exploiting coupling effects can yield essential information. For instance, the $^1H–^{31}P$ J-coupling detected in the new superprotonic solid acid $Cs_7(H_4PO_4)(H_2PO_4)_8$, enabled differentiation of conventional $(H_2PO_4)^-$ polyanion groups from the unusual polycation $(H_4PO_4)^+$.[121] Similarly, in $CsH(PO_3H)$, the acid proton is clearly distinguished from the covalently bonded hydrogen via the strong $^1H–^{31}P$ J-coupling detected for the latter, and these hydrogen species do not show site exchange even in the high-temperature superprotonic state.[141] In another example, $\{^{71}Ga\}$ [^1H] rotational echo double resonance experiments revealed Ga–H distances in a high-performance indium gallium oxide (IGO) thin-film transistor. The measured value of 3.4 Å excludes the possibility of Ga–H bonds and confirms the existence of Ga–OH instead.[142]

Multidimensional homonuclear or heteronuclear correlation NMR experiments are used to directly establish spatial proximities among various hydrogen species and between hydrogen and their hosts. For instance, $^1H–^{17}O$ correlation experiments based on J-coupling NMR interactions have been used to establish a quantitative correlation between the coupling strength (frequency) and the hydrogen and oxygen atomic distance.[143] Of relevance to perovskite proton conductors is the exploitation of magnetic dipolar interactions, in combination with dynamic nuclear polarization for signal enhancement, to study $^1H–^{89}Y$ proximity in Y-doped BZO.[144] These cross-polarization experiments confirmed earlier hypotheses regarding proton trapping in the vicinity of the dopant.[23] Among these methods, $^1H–^1H$ dipolar-coupling-driven spin diffusion NMR experiments are particularly valuable in determining the size of hydrogen-laden domains in multicomponent systems, a parameter often critical for understanding hydrogen diffusion.[145] In parallel with experimental efforts, *ab initio* simulations of NMR spectra often play a crucial role in aiding the interpretation of the data and establishing mechanistic insights.[146]

Determination of hydrogen and host dynamics

Beyond knowledge of the approximately static oxidation state and position of hydrogen in a structure, access to hydrogen dynamics, both local and long-range, is essential to understanding the influence of hydrogen on material properties. In some cases, the property of interest is the transport itself, as in proton conductivity, and in others, a secondary property such as the proton-modulated electronic conductivity or the anion exchange rate for hydride preparation is sought.

Neutron scattering

Hydrogen dynamics (fluctuation of atomic structure) can be measured with inelastic neutron scattering. Unlike diffraction, inelastic techniques rely on sensitivity to the incoherent
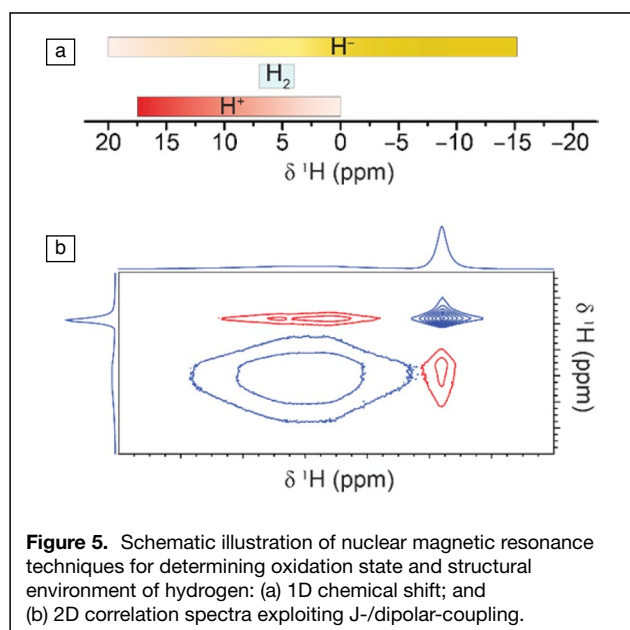

Figure 5. Schematic illustration of nuclear magnetic resonance techniques for determining oxidation state and structural environment of hydrogen: (a) 1D chemical shift; and (b) 2D correlation spectra exploiting J-/dipolar-coupling.

scattering cross section, which is about 80 times higher for ^{1}H than other atoms/isotopes, making these methods particularly suitable for characterizing the behavior of hydrogen in solids.[125] Inelastic neutron spectroscopy (INS) is more sensitive to hydrogen than Raman and infrared spectroscopy, has no optical selection rules, and is a bulk technique due to the deeply penetrating nature of neutrons. In materials with physisorption of hydrogen, INS can measure the rotational spectra of H_2 in its host lattice and distinguish between ortho- and para-hydrogen (**Figure 6**).[118] Advances in computational simulation have furthered techniques in INS, as the spectra can be directly modeled from a molecular dynamics simulation or phonon mode calculation to identify the active modes. INS experiments of the barium titanate oxyhydride showed that H^- ions locate on oxygen sites via measured TiH bending modes and complementary DFT calculations.[56] INS with complementary computer modeling and Fourier difference maps from neutron diffraction was used to identify both surface H and encaged hydride in a Ru-loaded electride clathrate (C12A7).[126]

Although local rotational motion of H_2 in a host can be measured with INS spectra, these methods do not generally have the energy resolution to characterize motion relevant to long-range diffusion. In contrast, the quasi-elastic region, the broadening around the elastic line at zero energy transfer, can give time-resolved information on diffusive motions in backscatter spectroscopy instruments that are optimized for low energy resolution. Quasi-elastic neutron scattering, similar to INS, is extremely sensitive ^{1}H and is useful to detect motions such as water molecule rotational and translational diffusion and diffusion of hydrogen through a lattice.[125,127]
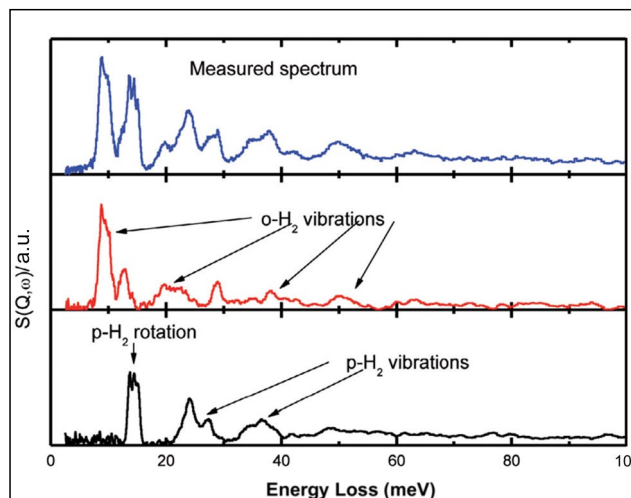

Figure 6. Vibrational spectra from inelastic neutron scattering is extremely sensitive to hydrogen and can distinguish para- and ortho-H_2 in a host such as ice clathrate, aided by computational models.[118] Reprinted with permission from Reference 118. © 2009 Elsevier.

NMR relaxometry and related transport measurements

Several NMR techniques[147] are available for probing proton dynamics at both the local and macroscopic length scales (**Figure 7**). [1]H spin relaxometry measurements, in which the diffusion-induced spin–lattice relaxation rate (SLR) $1/T_1$ is recorded, reveal intrinsic local ion mobility and dynamic correlations. The term T_1 depends on the residence time, τ_c, according to:
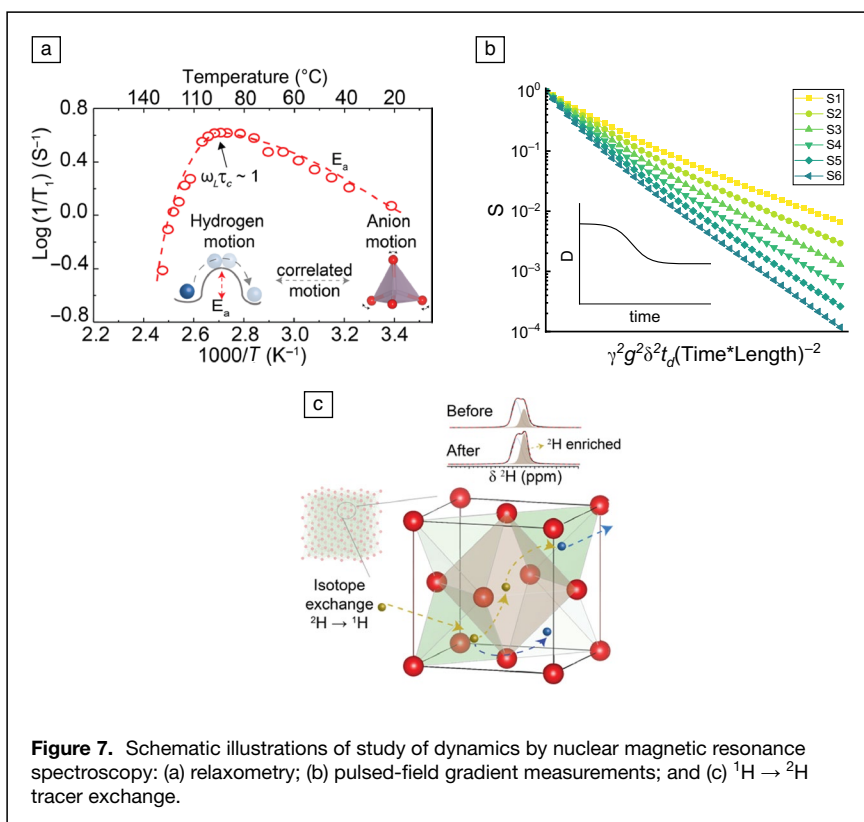
$$\frac{1}{T_1} = C \cdot \left(\frac{\tau_c}{1 + (\omega_L \tau_c)^\beta} + \frac{4\tau_c}{1 + (2\omega_L \tau_c)^\beta} \right), \qquad 1$$

where ω_L is the Larmor frequency, β is the dimensionality factor, and C is an approximately known constant. Generally, a dimensionality factor $\beta = 2$ indicates uncorrelated ion motion, whereas a β value between 1 and 2 suggests correlated ion motion.[148,149] When $\beta = 1$, Equation 1 reverts to the well-known Bloembergen–Purcell–Pound (BPP) expression, and the residence time can be determined. Variable-temperature measurements are typically employed in such studies, from which the activation energy associated with the relaxation behavior can be extracted, where $\tau_c = \tau_c^0 \exp\left(\frac{E_a}{RT}\right)$ (Figure 7a). Furthermore, with an estimate of the jump distance, r, the measured residence time can be converted to tracer diffusivity according to $D = \frac{r^2}{6\tau_c}$. Comparison to the macroscopic diffusivity implied by the conductivity via the Nernst–Einstein relation reveals whether the local relaxation detected by NMR governs the long-range transport. Such an approach has been applied to the superionic plastic phase of $[(CH_3)_4N]SCN$, where it was shown that the rotation of the $(CH_3)_4N^+$ cations (detected by ^{1}H NMR relaxometry) and the long-range ion transport (detected by AC conductivity measurement) occur with the same dynamics and hence via the same mechanism.[150]

At the mesoscopic scale, pulsed-field gradient (PFG) NMR can determine tracer diffusivities $D*$. In a PFG experiment, one exploits the fact that the measured signal amplitude relative to that without diffusion is a function of the diffusivity, $D*$, and of several experimentally tunable parameters: the gradient field strength, g, the duration of the applied gradient field, δ, and the interval between the two gradient pulses, Δ, and is given as[147,151]

$$S(g, \delta, t_d) = \exp\left(-\gamma^2 g^2 \delta^2 t_d D*\right), \qquad 2$$

where γ is the gyromagnetic ratio of the NMR isotope of interest and $t_d = \Delta - \frac{\delta}{3}$ is the effective diffusion time. The diffusivity $D*$ can thus be obtained by varying g, δ, or Δ (Figure 7b). If the diffusion occurs via multiple distinguishable microstructural components, Equation 2 is replaced by a summation reflecting the contribution of each component to the macroscopic behavior. The method requires long spin–spin relaxation times, a condition more often encountered in liquids and porous media than condensed solids. In the context of solid-state proton conductors, the application of PFG NMR has been largely focused on polymeric materials, where the microstructural

Figure 7. Schematic illustrations of study of dynamics by nuclear magnetic resonance spectroscopy: (a) relaxometry; (b) pulsed-field gradient measurements; and (c) $^1H \rightarrow {}^2H$ tracer exchange.

complexity provides particular motivation for exploiting the time- and length-scale resolution afforded by NMR methods. For example, PFG NMR has enabled resolution of two diffusional processes in composite materials, with regions in which water diffuses freely, with a diffusion coefficient similar to that of bulk water, and regions in which the water is highly bound, with a diminished diffusion coefficient.[148]

Though not yet demonstrated, $^1H \rightarrow {}^2H$ tracer-exchange NMR can, in principle, resolve the chemical/structural sites participating in hydrogen conduction and reveal hydrogen transport pathways on the atomic scale. During the tracer-exchange process, ^2H will partially replace ^1H on its migration pathways in the material systems of interest. Identifying and quantifying the $^2H \rightarrow {}^1H$ replacement sites will result in a map of hydrogen migration pathways (Figure 7c). We have used analogous $^6Li \rightarrow {}^7Li$ tracer-exchange experiments in Li ion conductors to determine ion transport pathways in inorganic,[152] organic, and hybrid ion conductors[153] and to establish the role of the interface in ion transport,[154] demonstrating the viability of the approach.

Outlook

This snapshot of research activities in the field of hydrogen-laden materials underscores exciting recent breakthroughs, remaining open questions, and breathtaking experimental tools now available for unveiling the nature of hydrogen in solid-state matter. Linking insights and measurements are decisive computational

efforts, spanning from the discovery of proton transport descriptors to *ab initio* prediction of INS and NMR spectra. While traditionally considered in the context of sustainable energy—still very much an important application for hydrogen—new areas are emerging in information science and fundamental control of electronic state. Combined with delivery of extreme stimuli to activate hydrogen response, untold innovative applications can be imagined.

Data availability

Not applicable.

Competing interests

On behalf of all authors, the corresponding author states that there is no conflict of interest.

References

1. S. Choi, T.C. Davenport, S.M. Haile, *Energy Environ. Sci.* **12**, 206 (2019)
2. F. Liu, H. Deng, D. Diercks, P. Kumar, M.H.A. Jabbar, C. Gumeci, Y. Furuya, N. Dale, T. Oku, M. Usuda, P. Kazempoor, L. Fang, D. Chen, B. Liu, C. Duan, *Nat. Energy* **8**, 1145 (2023)
3. C.C. Duan, R. Kee, H.Y. Zhu, N. Sullivan, L.Z. Zhu, L.Z. Bian, D. Jennings, R. O'Hayre, *Nat. Energy* **4**, 230 (2019)
4. X.H. Yao, K. Klyukin, W.J. Lu, M. Onen, S. Ryu, D. Kim, N. Emond, I. Waluyo, A. Hunt, J.A. del Alamo, J. Li, B. Yildiz, *Nat. Commun.* **11**, 10 (2020)
5. M. Huang, M. Schwacke, M. Onen, J. del Alamo, J. Li, B. Yildiz, *Adv. Mater.* **35**, 2205169 (2023)
6. M. Onen, N. Emond, B.M. Wang, D.F. Zhang, F.M. Ross, J. Li, B. Yildiz, J.A. del Alamo, *Science* **377**, 539 (2022)
7. Y. Kobayashi, O. Hernandez, C. Tassel, H. Kageyama, *Sci. Technol. Adv. Mater.* **18**, 905 (2017)
8. K.-D. Kreuer, *Chem. Mater.* **8**(3), 610 (1996)
9. C.J.T. Grotthuss, *Ann. Chim.* **58**, 54 (1806)
10. K.D. Kreuer, A. Rabenau, W. Weppner, *Angew. Chem. Int. Ed. Engl.* **21**, 208 (1982)
11. S.M. Haile, D.A. Boysen, C.R.I. Chisholm, R.B. Merle, *Nature* **410**, 910 (2001)
12. D.A. Boysen, T. Uda, C.R.I. Chisholm, S.M. Haile, *Science* **303**, 68 (2004)
13. S.M. Haile, C.R.I. Chisholm, K. Sasaki, D.A. Boysen, T. Uda, *Faraday Discuss.* **134**, 17 (2007)
14. K.D. Kreuer, *Annu. Rev. Mater. Res.* **33**, 333 (2003)
15. T. Chen, Y. Jing, L.O. Anderson, K. Leonard, H. Matsumoto, N. Aluru, N.H. Perry, *J. Phys. Chem. C* **125**, 26216 (2021)
16. E. Fabbri, D. Pergolesi, E. Traversa, *Chem. Soc. Rev.* **39**, 4355 (2010)
17. Y. Shin, Y.D. Kim, M. Sanders, S.P. Harvey, M. Walker, R. O'Hayre, *J. Mater. Chem. A* **10**, 24839 (2022)
18. S.M. Haile, *Mater. Today* **6**, 24 (2003)
19. A.I. Baranov, *Crystallogr. Rep.* **48**, 1012 (2003)
20. K.D. Kreuer, *Solid State Ionics* **94**, 55 (1997)
21. C. Dreßler, D. Sebastiani, *Phys. Chem. Chem. Phys.* **22**, 10738 (2020)
22. A. Ishikawa, H. Maekawa, T. Yamamura, Y. Kawakita, K. Shibata, M. Kawai, *Solid State Ionics* **179**, 2345 (2008)
23. Y. Yamazaki, F. Blanc, Y. Okuyama, L. Buannic, J.C. Lucio-Vega, C.P. Grey, S.M. Haile, *Nat. Mater.* **12**, 647 (2013)
24. A. Torayev, L. Sperrin, M.A. Gomez, J.A. Kattirtzi, C. Merlet, C.P. Grey, *J. Phys. Chem. C* **124**, 16689 (2020)
25. L.F. Zhang, F. Yao, J.L. Meng, W.W. Zhang, H.C. Wang, X.J. Liu, J. Meng, H.J. Zhang, *J. Mater. Chem. A* **7**, 18558 (2019)
26. S. Fop, *J. Mater. Chem. A* **9**, 18836 (2021)
27. N.P. Lu, Z. Zhang, Y.J. Wang, H.B. Li, S. Qiao, B. Zhao, Q. He, S.C. Lu, C. Li, Y.S. Wu, M.T. Zhu, X.Y. Lyu, X.K. Chen, Z.L. Li, M. Wang, J.Z. Zhang, S.C. Tsang, J.W. Guo, S.Z. Yang, J.B. Zhang, K. Deng, D. Zhang, J. Ma, J. Ren, Y. Wu, J.Y. Zhu, S.Y. Zhou, Y. Tokura, C.W. Nan, J. Wu, P. Yu, *Nat. Energy* **7**, 1208 (2022)
28. N. Bork, N. Bonanos, J. Rossmeisl, T. Vegge, *Phys. Rev. B* **82**, 6 (2010)
29. M.A. Gomez, M.A. Griffin, S. Jindal, K.D. Rule, V.R. Cooper, *J. Chem. Phys.* **123**, 10 (2005)
30. K.D. Kreuer, A. Fuchs, J. Maier, *Solid State Ionics* **77**, 157 (1995)
31. Y. Zhou, X.F. Guan, H. Zhou, K. Ramadoss, S. Adam, H.J. Liu, S. Lee, J. Shi, M. Tsuchiya, D.D. Fong, S. Ramanathan, *Nature* **534**, 231 (2016)
32. Z.L. Li, S.C. Shen, Z.J. Tian, K. Hwangbo, M. Wang, Y.J. Wang, F.M. Bartram, L.Q. He, Y.J. Lyu, Y.Q. Dong, G. Wan, H.B. Li, N.P. Lu, J.D. Zang, H. Zhou, E. Arenholz, Q. He, L.Y. Yang, W.D. Luo, P. Yu, *Nat. Commun.* **11**, 9 (2020)
33. C.Y. Jones, J. Wu, L.P. Li, S.M. Haile, *J. Appl. Phys.* **97**, 114908 (2005). https://doi.org/10.1063/1.1922590
34. N.P. Lu, P.F. Zhang, Q.H. Zhang, R.M. Qiao, Q. He, H.B. Li, Y.J. Wang, J.W. Guo, D. Zhang, Z. Duan, Z.L. Li, M. Wang, S.Z. Yang, M.Z. Yan, E. Arenholz, S.Y. Zhou, W.L. Yang, L. Gu, C.W. Nan, J. Wu, Y. Tokura, P. Yu, *Nature* **546**, 124 (2017)
35. Q. Zhao, L.J. Liu, J.F. Yin, J.X. Zheng, D.H. Zhang, J. Chen, L.A. Archer, *Angew. Chem. Int. Ed.* **59**, 3048 (2020)
36. O. Bohnke, C. Bohnke, B. Carquille, *Vide Sci. Tech. Appl.* **37**, 403 (1982)
37. M.S. Islam, S. Wang, A.M. Nolan, Y.F. Mo, *Chem. Mater.* **33**, 8278 (2021)
38. M.S. Islam, S. Wang, A.T. Hall, Y.F. Mo, *Chem. Mater.* **11**, 1 (2022)
39. F.M. Draber, C. Ader, J.P. Arnold, S. Eisele, S. Grieshammer, S. Yamaguchi, M. Martin, *Nat. Mater.* **19**, 577 (2020)
40. F.M. Draber, C. Ader, J.P. Arnold, S. Eisele, S. Grieshammer, S. Yamaguchi, M. Martin, *Nat. Mater.* **19**, 338 (2020)
41. Y.Q. Meng, J. Gao, Z.Y. Zhao, J. Amoroso, J.H. Tong, K.S. Brinkman, *J. Mater. Sci.* **54**, 9291 (2019)
42. K.D. Kreuer, *Solid State Ionics* **136**, 149 (2000)
43. K. Wakamura, *Solid State Ionics* **180**, 1343 (2009)
44. X.Y. Li, N.A. Benedek, *Chem. Mater.* **27**, 2647 (2015)
45. S. Muy, J.C. Bachman, L. Giordano, H.H. Chang, D.L. Abernathy, D. Bansal, O. Delaire, S. Hori, R. Kanno, F. Maglia, S. Lupart, P. Lamp, Y. Shao-Horn, *Energy Environ. Sci.* **11**, 850 (2018)
46. W. Munch, K.D. Kreuer, J. Maier, G. Seifert, "Comparison of Proton Migration Energies of the Perovskites $BaTiO_3$, $BaZrO_3$, and $BaCeO_3$ by Quantum Molecular

Dynamics," in *Proceedings of the Fifth International Symposium on Solid Oxide Fuel Cells (SOFC-V)* (Electrochemical Society, Pennington, 1997), p. 1203
47. W. Munch, G. Seifert, K.D. Kreuer, J. Maier, *Solid State Ionics* **86–8**, 647 (1996)
48. K. Wakamura, *J. Phys. Chem. Solids* **66**, 133 (2005)
49. M.C. Verbraeken, C. Cheung, E. Suard, J.T.S. Irvine, *Nat. Mater.* **14**, 95 (2015)
50. G.J. Irvine, F. Demmel, H.Y. Playford, G. Carins, M.O. Jones, J.T.S. Irvine, *Chem. Mater.* **34**, 9934 (2022)
51. K. Fukui, S. Iimura, A. Iskandarov, T. Tada, H. Hosono, *J. Am. Chem. Soc.* **144**, 1523 (2022)
52. K. Fukui, S. Iimura, T. Tada, S. Fujitsu, M. Sasase, H. Tamatsukuri, T. Honda, K. Ikeda, T. Otomo, H. Hosono, *Nat. Commun.* **10**, 8 (2019)
53. Y. Kobayashi, O.J. Hernandez, T. Sakaguchi, T. Yajima, T. Roisnel, Y. Tsujimoto, M. Morita, Y. Noda, Y. Mogami, A. Kitada, M. Ohkura, S. Hosokawa, Z.F. Li, K. Hayashi, Y. Kusano, J.E. Kim, N. Tsuji, A. Fujiwara, Y. Matsushita, K. Yoshimura, K. Takegoshi, M. Inoue, M. Takano, H. Kageyama, *Nat. Mater.* **11**, 507 (2012)
54. T. Yajima, A. Kitada, Y. Kobayashi, T. Sakaguchi, G. Bouilly, S. Kasahara, T. Terashima, M. Takano, H. Kageyama, *J. Am. Chem. Soc.* **134**, 8782 (2012)
55. X. Liu, T.S. Bjørheim, L. Vines, Ø.S. Fjellvåg, C. Granerød, Ø. Prytz, T. Yamamoto, H. Kageyama, T. Norby, R. Haugsrud, *J. Am. Chem. Soc.* **141**, 4653 (2019)
56. C. Eklöf-Österberg, L. Mazzei, E.J. Granhed, G. Wahnström, R. Nedumkandathil, U. Häussermann, A. Jaworski, A.J. Pell, S.F. Parker, N.H. Jalarvo, L. Börjesson, M. Karlsson, *J. Mater. Chem. A* **8**, 6360 (2020)
57. G.J. Irvine, R.I. Smith, M.O. Jones, J.T.S. Irvine, *Nat. Commun.* **14**, 8 (2023)
58. S.M. Haile, D.L. West, J. Campbell, *J. Mater. Res.* **13**, 1576 (1998)
59. R.A. De Souza, Z.A. Munir, S. Kim, M. Martin, *Solid State Ionics* **196**, 1 (2011)
60. S. Choi, C.J. Kucharczyk, Y.G. Liang, X.H. Zhang, I. Takeuchi, H.I. Ji, S.M. Haile, *Nat. Energy* **3**, 202 (2018)
61. W. Bian, W. Wu, B. Wang, W. Tang, M. Zhou, C. Jin, H. Ding, W. Fan, Y. Dong, J. Li, D. Ding, *Nature* **604**, 479 (2022)
62. C. Li, X. Tong, C. Yuan, Y. Tong, Y. Zhang, N. Wang, P. Li, S. Pang, L. Wang, Z. Zhan, *Ceram. Int.* **50**, 4656 (2024)
63. X.W. Sun, E. Vollestad, P.M. Rorvik, S. Prodinger, G.N. Kalantzopoulos, A. Chatzitakis, T. Norby, *Appl. Surf. Sci.* **611**, 12 (2023)
64. P. Lejček, "Grain Boundaries: Description, Structure and Thermodynamics," in *Grain Boundary Segregation in Metals*, ed. by P. Lejcek (Springer, Berlin, 2010), p. 5
65. T. Chen, G.F. Harrington, J. Matsuda, K. Sasaki, D. Pham, E.L. Corral, N.H. Perry, *J. Electrochem. Soc.* **166**, F569 (2019)
66. G. Gregori, R. Merkle, J. Maier, *Prog. Mater Sci.* **89**, 252 (2017)
67. X. Tong, D.S. Mebane, R.A. De Souza, *J. Am. Ceram. Soc.* **103**, 5 (2020)
68. D.A. Boysen, S.M. Haile, H.J. Liu, R.A. Secco, *Chem. Mater.* **15**, 727 (2003)
69. S. Kim, H.J. Avila-Paredes, S. Wang, C.-T. Chen, R.A. De Souza, M. Martin, Z.A. Munir, *Phys. Chem. Chem. Phys.* **11**, 3035 (2009)
70. C. Tandé, D. Pérez-Coll, G.C. Mather, *J. Mater. Chem.* **22**, 11208 (2012)
71. A. Lindman, E.E. Helgee, G. Wahnström, *Chem. Mater.* **29**, 7931 (2017)
72. F. Iguchi, N. Sata, H. Yugami, *J. Mater. Chem.* **20**, 6265 (2010)
73. C. Kjolseth, H. Fjeld, O. Prytz, P.I. Dahl, C. Estournès, R. Haugsrud, T. Norby, *Solid State Ionics* **181**, 268 (2010)
74. T. Bondevik, J.M. Polfus, T. Norby, *Solid State Ionics* **353**, 115369 (2020)
75. Y. Yamazaki, R. Hernandez-Sanchez, S.M. Haile, *Chem. Mater.* **21**, 2755 (2009)
76. P. Babilo, S.M. Haile, *J. Am. Ceram. Soc.* **88**, 2362 (2005)
77. E. Kim, Y. Yamazaki, S.M. Haile, H.I. Yoo, *Solid State Ionics* **275**, 23 (2015)
78. S.W. Tao, J.T.S. Irvine, *Adv. Mater.* **18**, 1581 (2006)
79. Y. Huang, R. Merkle, J. Maier, *Solid State Ionics* **347**, 115256 (2020)
80. D.R. Clark, D.R. Diercks, S. Ricote, T.T. Dearden, N.P. Sullivan, J.W. Medlin, B.P. Gorman, R.P. O'Hayre, *J. Mater. Chem. C* **11**, 5082 (2023)
81. A.K. Baral, Y. Tsur, *J. Am. Ceram. Soc.* **102**, 239 (2019)
82. Z.Q. Sun, E. Fabbri, L. Bi, E. Traversa, *Phys. Chem. Chem. Phys.* **13**, 7692 (2011)
83. S.N. Rashkeev, D.M. Fleetwood, R.D. Schrimpf, S.T. Pantelides, *Appl. Phys. Lett.* **81**, 1839 (2002)
84. N.H. Perry, *Local Electrical and Dielectric Properties of Nanocrystalline Solid Oxide Fuel Cell Electrolytes* (Northwestern University, Evanston, 2009)
85. S.Ø. Stub, E. Vøllestad, T. Norby, *J. Phys. Chem. C* **121**, 12817 (2017)
86. T. Bayer, S.R. Bishop, N.H. Perry, K. Sasaki, S.M. Lyth, *ACS Appl. Mater. Interfaces* **8**, 11466 (2016)
87. S. Miyoshi, Y. Akao, N. Kuwata, J. Kawamura, Y. Oyama, T. Yagi, S. Yamaguchi, *Chem. Mater.* **26**, 5194 (2014)
88. M. Shirpour, G. Gregori, R. Merkle, J. Maier, *Phys. Chem. Chem. Phys.* **13**, 937 (2011)
89. T.-S. Oh, D.A. Boyd, D.G. Goodwin, S.M. Haile, *Phys. Chem. Chem. Phys.* **15**, 2466 (2013)
90. J. Gu, L. Jiang, S.A. Ismail, H. Guo, D. Han, *Adv. Mater. Interfaces* **10**, 2201764 (2023)
91. M. Nogami, Y. Tarutani, Y. Daiko, S. Izuhara, T. Nakao, T. Kasuga, *J. Electrochem. Soc.* **151**, A2095 (2004)
92. S. Prakash, W.E. Mustain, S. Park, P.A. Kohl, *J. Power Sources* **175**, 91 (2008)
93. S.T. Wang, H. Jiang, Y.H. Dong, D. Clarkson, H. Zhu, C.M. Settens, Y. Ren, T. Nguyen, F. Han, W.W. Fan, S.Y. Kim, J.A. Zhang, W.J. Xue, S.K. Sandstrom, G.Y. Xu, E. Tekoglu, M.D. Li, S.L. Deng, Q. Liu, S.G. Greenbaum, X.L. Ji, T. Gao, J. Li, *Adv. Mater.* **34**, 10 (2022)
94. S.O. Stub, K. Thorshaug, P.M. Rorvik, T. Norby, E. Vollestad, *Phys. Chem. Chem. Phys.* **20**, 15653 (2018)

95. X.L. Kang, A. Chatzitakis, T. Aarholt, X.W. Sun, C. Negri, T. Norby, *J. Mater. Chem. A* **10**, 218 (2021)

96. C. Zhao, Y. Li, W. Zhang, Y. Zheng, X. Lou, B. Yu, J. Chen, Y. Chen, M. Liu, J. Wang, *Energy Environ. Sci.* **13**, 53 (2020)

97. M.D. Armstrong, K.-W. Lan, Y. Guo, N.H. Perry, *ACS Nano* **15**, 9211 (2021)

98. N. Yang, C. Cantoni, V. Foglietti, A. Tebano, A. Belianinov, E. Strelcov, S. Jesse, D. Di Castro, E. Di Bartolomeo, S. Licoccia, S.V. Kalinin, G. Balestrino, C. Aruta, *Nano Lett.* **15**, 2343 (2015)

99. C. Xia, Y. Mi, B. Wang, B. Lin, G. Chen, B. Zhu, *Nat. Commun.* **10**, 1707 (2019)

100. Y. Xing, B. Zhu, L. Hong, C. Xia, B. Wang, Y. Wu, H. Cai, S. Rauf, J. Huang, M.I. Asghar, Y. Yang, W.-F. Lin, *ACS Appl. Energy Mater.* **5**, 15373 (2022)

101. Q. Su, D. Yoon, A. Chen, F. Khatkhatay, A. Manthiram, H. Wang, *J. Power Sources* **242**, 455 (2013)

102. B. Yildiz, *MRS Bull.* **39**(2), 147 (2014)

103. H. Aydin, C. Korte, M. Rohnke, J. Janek, *Phys. Chem. Chem. Phys.* **15**, 1944 (2013)

104. W.D. Shen, J. Jiang, J.L. Hertz, *RSC Adv.* **4**, 21625 (2014)

105. A. Fluri, D. Pergolesi, V. Roddatis, A. Wokaun, T. Lippert, *Nat. Commun.* **7**, 9 (2016)

106. A. Kushima, B. Yildiz, *J. Mater. Chem.* **20**, 4809 (2010)

107. J. Wei, D. Ogawa, T. Fukumura, Y. Hirose, T. Hasegawa, *Cryst. Growth Des.* **15**, 2187 (2015)

108. P. Žguns, B. Yildiz, *PRX Energy* **1**, 023003 (2022)

109. Q.L. Chen, A. Braun, S. Yoon, N. Bagdassarov, T. Graule, *J. Eur. Ceram. Soc.* **31**, 2657 (2011)

110. A. Fluri, A. Marcolongo, V. Roddatis, A. Wokaun, D. Pergolesi, N. Marzari, T. Lippert, *Adv. Sci.* **4**, 10 (2017)

111. J. Hyodo, Y. Yamazaki, *J. Phys. Energy* **4**, 16 (2022)

112. Z.J. Fan, N.N. Li, P. Du, W.G. Yang, Q.L. Chen, *J. Phys. Chem. C* **124**, 22376 (2020)

113. R.W. Balluffi, S.M. Allen, W.C. Carter, R.A. Kemper, *Kinetics of Materials* (Wiley, Hoboken, 2005), p. 55

114. M. Youssef, K.J. Van Vliet, B. Yildiz, *Phys. Rev. Lett.* **119**, 6 (2017)

115. T. Defferriere, D. Klotz, J.C. Gonzalez-Rosillo, J.L.M. Rupp, H.L. Tuller, *Nat. Mater.* **21**, 438 (2022)

116. T.Y. Wei, K.L. Lim, Y.S. Tseng, S.L.I. Chan, *Renew. Sustain. Energy Rev.* **79**, 1122 (2017)

117. S. de Graaf, J. Momand, C. Mitterbauer, S. Lazar, B.J. Kooi, *Sci. Adv.* **6**, 4312 (2020)

118. A.J. Ramirez-Cuesta, M.O. Jones, W.I.F. David, *Mater. Today* **12**, 54 (2009)

119. C. Sun, C. Wang, T. Ha, J. Lee, J.H. Shim, Y. Kim, *Nano Energy* **113**, 108554 (2023)

120. G. Kim, F. Blanc, Y.Y. Hu, C.P. Grey, *J. Phys. Chem. C* **117**, 6504 (2013)

121. L.S. Wang, S.V. Patel, S.S. Sanghvi, Y.Y. Hu, S.M. Haile, *J. Am. Chem. Soc.* **142**, 19992 (2020)

122. Z.H. Zhu, V. Shutthanandan, M. Engelhard, *Surf. Interface Anal.* **44**, 232 (2012)

123. K. Takaba, S. Maki-Yonekura, I. Inoue, K. Tono, T. Hamaguchi, K. Kawakami, H. Naitow, T. Ishikawa, M. Yabashi, K. Yonekura, *Nat. Commun.* **15**, 491 (2023)

124. M.T.B. Clabbers, T. Gruene, E.V. Genderen, J.P. Abrahams, *Acta Crystallogr. Sect. A Found. Adv.* **75**, 82 (2019)

125. G. Schirò, *EPJ Web Conf.* **236**, 05001 (2020)

126. J. Kammert, J. Moon, Y. Cheng, L. Daemen, S. Irle, V. Fung, J. Liu, K. Page, X. Ma, V. Phaneuf, J. Tong, A.J. Ramirez-Cuesta, Z. Wu, *J. Am. Chem. Soc.* **142**, 7655 (2020)

127. F. Wang, H.A. Evans, K. Kim, L. Yin, Y. Li, P.-C. Tsai, J. Liu, S.H. Lapidus, C.M. Brown, D.J. Siegel, Y.-M. Chiang, *Chem. Mater.* **32**, 8481 (2020)

128. G. Kobayashi, Y. Hinuma, S. Matsuoka, A. Watanabe, M. Iqbal, M. Hirayama, M. Yonemura, T. Kamiyama, I. Tanaka, R. Kanno, *Science* **351**, 1314 (2016)

129. D.S. Charles, M. Feygenson, K. Page, J. Neuefeind, W. Xu, X. Teng, *Nat. Commun.* **8**, 15520 (2017)

130. K. Page, T. Proffen, M. Niederberger, R. Seshadri, *Chem. Mater.* **22**, 4386 (2010)

131. J. Liu, L. Yu, E. Hu, B.S. Guiton, X.-Q. Yang, K. Page, *Inorg. Chem.* **57**, 6873 (2018)

132. D.A. Keen, D.S. Keeble, T.D. Bennett, *Phys. Chem. Miner.* **45**, 333 (2018)

133. P.C. Tsai, S. Mair, J. Smith, D.M. Halat, P.H. Chien, K. Kim, D.H. Zhang, Y.L. Li, L. Yin, J. Liu, S.H. Lapidus, J.A. Reimer, N.P. Balsara, D.J. Siegel, Y.M. Chiang, *Adv. Energy Mater.* **13**, 10 (2023)

134. B.R. Cladek, S.M. Everett, M.T. McDonnell, D.G. Kizzire, M.G. Tucker, D.J. Keffer, C.J. Rawn, *Fuel* **299**, 8 (2021)

135. B.R. Cladek, S.M. Everett, M.T. McDonnell, M.G. Tucker, D.J. Keffer, C.J. Rawn, *Commun. Chem.* **4**, 7 (2021)

136. S.M. Everett, C.J. Rawn, B.C. Chakoumakos, D.J. Keefer, A. Huq, T.J. Phelps, *Am. Miner.* **100**, 1203 (2015)

137. Y. RuizMorales, G. Schreckenbach, T. Ziegler, *Organometallics* **15**, 3920 (1996)

138. K. Hayashi, P.V. Sushko, Y. Hashimoto, A.L. Shluger, H. Hosono, *Nat. Commun.* **5**, 8 (2014)

139. X.Y. Xue, M. Kanzaki, *J. Am. Ceram. Soc.* **92**, 2803 (2009)

140. A. Rankin, F. Pourpoint, N. Duong, L. Delevoye, J.-P. Amoureux, O. Lafon, "Advances in the Characterization of Inorganic Solids Using NMR Correlation Experiments," in *Comprehensive Inorganic Chemistry III*, 3rd edn., ed. by J. Reedijk, K.R. Poeppelmeier (Elsevier, Oxford, 2023), p. 534

141. G. Kim, J.M. Griffin, F. Blanc, D.M. Halat, S.M. Haile, C.P. Grey, *J. Phys. Chem. C* **121**, 27830 (2017)

142. W. Huang, P.H. Chien, K. McMillen, S. Patel, J. Tedesco, L. Zeng, S. Mukherjee, B.H. Wang, Y. Chen, G. Wang, Y. Wang, Y.S. Gao, M.J. Bedzyk, D.M. DeLongchamp, Y.Y. Hu, J.E. Medvedeva, T.J. Marks, A. Facchetti, *Proc. Natl. Acad. Sci. U.S.A.* **117**, 18231 (2020)

143. S.L. Carnahan, B.J. Lampkin, P. Naik, M.P. Hanrahan, I.I. Slowing, B. VanVeller, G. Wu, A.J. Rossini, *J. Am. Chem. Soc.* **141**, 441 (2019)

144. F. Blanc, L. Sperrin, D. Lee, R. Dervisoglu, Y. Yamazaki, S.M. Haile, G. De Paepe, C.P. Grey, *J. Phys. Chem. Lett.* **5**, 2431 (2014)

145. Y.-Y. Hu, Y. Yusufoglu, M. Kanapathipillai, C.-Y. Yang, Y. Wu, P. Thiyagarajan, T. Deming, M. Akinc, K. Schmidt-Rohr, S. Mallapragada, *Soft Matter* **5**, 4311 (2009)

146. A.C. Castro, D. Balcells, M. Repisky, T. Helgaker, M. Cascella, *Inorg. Chem.* **59**, 17509 (2020)

147. V.I. Volkov, A.A. Marinin, *Russ. Chem. Rev.* **82**(3), 248 (2013)

148. V.M. Bouznik, E.V. Morozov, I.A. Avilova, V.I. Volkov, *Appl. Magn. Reson.* **47**(3), 321 (2016)

149. L.D. Bustard, *Phys. Rev. B* **22**(1), 1 (1980)

150. T. Tanabe, D. Nakamura, R. Ikeda, *J. Chem. Soc. Faraday Trans.* **87**, 987 (1991)

151. C.S. Johnson, *Prog. Nucl. Magn. Reson. Spectrosc.* **34**, 203 (1999)

152. P. Wang, S. Patel, H. Liu, P.-H. Chien, X. Feng, L. Gao, B. Chen, J. Liu, Y.-Y. Hu, *Adv. Funct. Mater.* **33**, 2307954 (2023)

153. C. Yang, Q. Wu, W. Xie, X. Zhang, A. Brozena, J. Zheng, M.N. Garaga, B.H. Ko, Y. Mao, S. He, Y. Gao, P. Wang, M. Tyagi, F. Jiao, R. Briber, P. Albertus, C. Wang, S. Greenbaum, Y.-Y. Hu, A. Isogai, M. Winter, K. Xu, Y. Qi, L. Hu, *Nature* **598**, 590 (2021)

154. J. Zheng, M. Tang, Y.-Y. Hu, *Angew. Chem. Int. Ed.* **55**, 12538 (2016) □

Publisher's note

Heejung W. Chung is a doctoral candidate in materials science and engineering at the Massachusetts Institute of Technology, supported by the National Science Foundation Graduate Research Fellowship Program. She received a BS degree in computer science from Stanford University in 2021, and a MPhil degree in computational methods for materials science as a Gates Cambridge Scholar in 2022. Her research focuses on modeling proton transport in oxides, and she is particularly interested in understanding lattice dynamical effects. Chung can be reached by email at hjwchung@mit.edu.

Bernadette Cladek is a postdoctoral research associate in the Materials Science and Engineering Department at The University of Tennessee. She received her BS degree in ceramic engineering in 2015 from the New York State College of Ceramics at Alfred University, and her PhD degree in materials science and engineering from The University of Tennessee in 2020. Her research focuses on the crystal structure, properties, and local atomic disorder of materials using neutron and x-ray scattering combined with computational approaches to data analysis. Cladek can be reached by email at bcladek@utk.edu.

Yong-Yun Hsiau is a doctoral candidate in the Department of Materials Science and Engineering at the University of Illinois Urbana-Champaign. She received her BS degree from the College of Engineering at National Tsing Hua University, Taiwan, in 2022. Her research focuses on proton transport in solid-state ionic materials for fuel cells, with a particular emphasis on vertically aligned nanocomposite thin films. Hsiau can be reached by email at yhsiau2@illinois.edu.
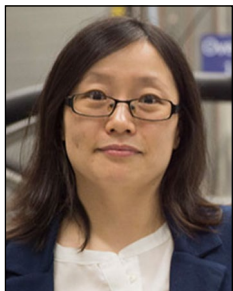
Yan-Yan Hu is a chemistry and biochemistry professor at Florida State University (FSU). She received her BS degree in chemistry from Tsinghua University, China, in 2006, and her PhD degree in analytical chemistry from Iowa State University in 2011. She worked as a Royal Society Newton Fellow and Marie Curie Research Fellow at the University of Cambridge, UK, from 2011 to 2014 before joining FSU and the National High Field Magnetic Laboratory in 2014. Her research specializes in advanced solid-state NMR techniques for studying functional materials. Hu can be reached by email at yhu@fsu.edu.

Katharine Page is an assistant professor in the Department of Materials Science and Engineering at The University of Tennessee, Knoxville, and a Joint Faculty member with the Neutron Scattering Division at Oak Ridge National Laboratory. She works at the intersection of energy materials research and the advancement of x-ray and neutron scattering methods. She is a recipient of the National Science Foundation CAREER Award, the US Department of Energy Office of Science Early Career Award, and Presidential Early Career Award for Scientists and Engineers. Page can be reached by email at kpage10@utk.edu.

Nicola H. Perry is an associate professor in the Department of Materials Science and Engineering at the University of Illinois Urbana-Champaign (UIUC). Her research addresses defect-informed design and discovery of solid-state ionic materials for energy applications (fuel cells, electrolyzers, all-solid-state batteries). Her awards include the National Science Foundation CAREER Award, the US Department of Energy Office of Science Early Career Award, The American Ceramic Society Richard M. Fulrath and Edward C. Henry Awards, The Electrochemical Society J. Bruce Wagner Jr. Award, and UIUC Dean's Award for Excellence in Research. Perry can be reached by email at nhperry@illinois.edu.

Bilge Yildiz is the Breene M. Kerr (1951) Professor at the Massachusetts Institute of Technology, where she leads the Laboratory for Electrochemical Interfaces. Her research focuses on laying the scientific groundwork to enable next-generation electrochemical devices for energy conversion and information processing. Her awards include the National Science Foundation CAREER Award, The Electrochemical Society Charles Tobias Young Investigator, and The American Ceramic Society Ross Coffin Purdy Awards. She is a Fellow of the American Physical Society, the Royal Society of Chemistry, and The Electrochemical Society, and a member of the Austrian Academy of Sciences. Yildiz can be reached by email at byildiz@mit.edu.

Sossina M. Haile holds a Murphy Professor Chair position in the Department of Materials Science and Engineering at Northwestern University, where she currently serves as the director of the Energy Frontiers Research Center on "Hydrogen in Energy and Information Sciences." Her research broadly encompasses materials for sustainable electrochemical energy technologies. She is the recipient of numerous awards, including a National Science Foundation American Competitiveness Initiative Fellowship and a Materials Research Society (MRS) David Turnbull Lectureship. She is a Fellow of MRS, the Royal Society of Chemistry, The American Ceramic Society, the African Academy of Sciences, and the Ethiopian Academy of Sciences. Haile can be reached by email at sossina.haile@northwestern.edu.